Pergamon

PII: S0042-6989(96)00001-6

Vision Res., Vol. 36, No. 15, pp. 2229–2247, 1996

Printed in Great Britain
0042-6989/96 $15.00 + 0.00

The Pathways of Light Measured in Fundus Reflectometry

JAN van de KRAATS,*† TOS T. J. M. BERENDSCHOT,† DIRK van NORREN†‡

Received 1 December 1994; in revised form 21 April 1995; in final form 13 December 1995

We measured the spectral reflectance of the fovea of ten normal subjects in four conditions, i.e. under dark-adapted and bleached conditions and at two retinal angles of incidence. The objective was to study optical pathways through the photoreceptor layer, resulting in a model that simultaneously explains spectral, directional and bleaching properties of the fovea. On theoretical grounds, we propose that small reflections from the stack of discs in the cone outer segments are the origin of the directional component of foveal reflection. Non-directional reflection occurs at the inner limiting membrane and at all layers posterior to the outer segments. With four reflectance spectra as input, the model allows determination of the density of the photostable absorbers, the lens, macular pigment, melanin and blood. Because of the simplified modeling of the layers posterior to the photoreceptor layer, the values for the density of melanin and blood are not necessarily comparable to physiological data. The density of the visual pigment calculated with this model is consistent with psychophysical data, with estimates for the ten subjects ranging from 0.41 to 0.80. The long wavelength sensitive cone fraction is calculated as 0.56. Copyright © 1996 Elsevier Science Ltd.

Density Directional Photoreceptor Reflectometry Stiles–Crawford

INTRODUCTION

Knowledge of the pathways light takes through the photoreceptor layer is important for understanding a number of phenomena such as the psychophysical Stiles–Crawford effect and the related directional reflex. Also, light that is not guided through the outer segments of the receptor does not lead to a catch in visual pigment. Retinal densitometry, a technique to assess the amount of visual pigment *in vivo*, is based on a comparison between the optical reflectance of the fundus in light- and dark-adapted states. The pathways that light takes through the receptor layer influence the calculation of the real amount of visual pigment. Rushton (1965) and Ripps & Weale (1965) made an early attempt to construct models to calculate the amount of visual pigment. The simplest model assumes (1) a homogeneous layer of light-absorbing visual pigment in the dark-adapted eye, (2) that this layer is transparent in the light-adapted state, (3) and that all light is reflected from a layer posterior to the pigment layer. The light thus passes the visual pigment in the outer segments of the photoreceptor twice. An important development of the simple model was the addition of light reflected anterior to the pigment layer, for instance at the internal limiting membrane (ILM). Rushton (1965) called this "superficial stray-light". A second type of stray-light, traveling through parallel pathways in the receptor interspaces, was called "fundal stray-light". The simple model, which ignores stray-light, underestimates the density of the visual pigment. However, the assessment of the amount of stray-light, and consequently the true density of the visual pigment, has remained a problem for 30 years. Low fractions of stray-light (2% at 500 nm) were found by Rushton (1965), whereas higher fractions of stray-light were reported by Ripps & Weale (1965) (33%) and King-Smith (1973a, b) (57%). The model of van Blokland & van Norren (1986), which is based on measurements of the directional reflection of the retina, added pathways of light in and around the receptor layer. This model predicted 50% stray-light.

Pathways of light can also be derived from models describing the absolute optical reflectance of the fundus. With the assumption that there are certain reflecting layers and a limited number of absorbers with known spectral extinction in the eye, these models try to quantify these layers by decomposing the measured spectrum. For reasons of simplicity, existing models used light levels

*To whom all correspondence should be addressed.
†Helmholtz Institute, Department of Ophthalmology E03. 136, Academic Hospital Utrecht, P.O. Box 85500, NL-3508 GA, Utrecht, The Netherlands.
‡Netherlands Aerospace Medical Centre, Kampweg 3, NL-3769 DE, Soesterberg, The Netherlands.

that were high enough to bleach the visual pigments. The implicit assumption is that the receptor layer is then completely transparent and can be ignored. Van Norren & Tiemeijer (1986) proposed a model with reflectance at two layers, the retinal pigment epithelium (RPE) and the sclera. Delori & Pflibsen (1989) expanded the model, incorporating more complex light scattering in the choroid.

The optical coherence technique applied to the retina provides a more direct way to study optical pathways (Huang *et al.*, 1991; Hitzenberger, 1991; Puliafito *et al.*, 1995; Hee *et al.*, 1995). Strong reflections (high amplitudes) are supposed to originate in the region of the choriocapillaris and the RPE. However, structures that scatter diffusely over a certain depth-range are less pronounced. We think that the present interpretation of OCT data leaves room for alternatives (c.f. Discussion).

Our aim was to derive a foveal reflection model that simultaneously explains spectral and directional reflection and bleaching effects. Within this rather complicated framework, it serves to first outline our main assumptions, and point out where they differ from existing models. Cone photoreceptors have a directionality that expresses itself in both the psychophysical Stiles–Crawford effect (Stiles & Crawford, 1933) and directional reflection (van Blokland, 1986). How do the directional properties of the receptor layer influence light reflected from deeper layers? On the basis of the nature of the diffuse white sclera and the multiple scattering of light by the choroidal tissues, we assume that the deeper layers taken together act to some extent as a diffuser with non-directional properties. Optical theory states that looking at a perfect diffuser through refracting optics (for instance a lens or in our case bleached photoreceptors), yields the same apparent reflectance as there would be without these optical elements (Longhurst, 1973). This is because the concentration (amplification of vergency) of light at entry is exactly nullified in the reverse pathway. The reflectivity of the perfect diffuser is constant for all angles, only for very large angles the amplification of vergency yields angles over 90 deg, and prevents light from reaching the diffuser.

Another approach leading to the same conclusion is that all light from a certain retinal angle, either going (partly) through the bleached outer segment or going through the interspaces, enters the deeper layers, forming a three-dimensional cloud of diffuse deeper light. Whereas with different retinal angles, the fractions of light traveling through the outer segments and the interspaces may change, the intensity of the deeper cloud of light remains constant. If a fixed relation exists between entrance light and light posterior to the receptor layer, this relation also must hold for the reverse pathway (reciprocity principle), and consequently emerging light going back from the deeper layers to the direction of the entering light cannot show directionality. This view eliminates the difficult problem of how to divide light entering the receptor layer from the scleral side, into a part entering the outer segments (with strong directionality) and a part entering the receptor interspaces (with, at first sight, non-directional behavior).

If, as argued above, the structures beyond the (bleached) receptor layer do not show directional effects, there must be other sources for the origin of light with directional behavior. As we know from the measurements of van Blokland & van Norren (1986), dark adaptation of the eye (resulting in increased absorption in the visual pigments) greatly reduces the magnitude of the directional component. This eliminates all sources of the directional reflex anterior to the outer segments of the receptors. The only remaining candidate for the origin of the directional reflex, in our view, then lies in the outer segment layer itself, in particular in the cone photoreceptor discs. For anatomical and optical reasons, we are unable to identify other structures that could fulfil this function. The index of refraction of the disc material (1.43) is higher than the fluid around it (1.36) (Piket-May *et al.*, 1993). Fresnel reflection for this index of refraction step cannot be directly applied due to the small dimension of the thickness of the discs (about 15 nm) compared to the wavelength. More appropriate in this case would be thin film reflection theory (Longhurst, 1973), whereby interference of the reflection at the back of the disc would largely compensate for the reflection at the front, leaving a very small residual reflection. However, the accumulation of about a thousand of these tiny disc reflections may be substantial. Evidence for reflection from the stack of discs comes from a technique which shows the existence of a standing wave pattern in a receptor model, by solving the time integrated Maxwell equations. This technique, however, is still in its infancy and calculations require considerable time on a super computer (Piket-May *et al.*, 1993). As the magnitude of the reflection of the discs depends on many questionable and unknown variables, the only assumption we make for our model is that there is a given reflection from the discs.

The model presented here is the first to our knowledge to incorporate the receptor layer into a reflection model of the human fovea, assuming directional reflection from the stack of discs in the outer segments and non-directional reflection from pre-retinal and post-retinal layers. Our approach thus differs from previous studies that relied on a directional reflection from origins posterior to the receptor layer (van Blokland & van Norren, 1986; Delori & Pflibsen, 1989; Gorrand & Delori, 1995). We used the model to estimate the proportions of light in the optical pathways passing the photolabile visual pigments twice, partly twice or not at all. Estimates for the density of the visual pigments were obtained that are consistent with psychophysical data.

METHODS

Experimental setup

Fundus reflection measurements were performed with a slightly modified version of the Utrecht Retinal Densitometer (van Norren & van de Kraats, 1989). A few essential details are presented below. The instrument

enables, in contrast with older type densitometers, investigation of the directional effects of the photoreceptors, by moving a fixed configuration of small, and closely spaced entry and exit pupils, over the subject's pupil. The small entry and exit pupils further ensured minimal contribution of reflections from the instrument's output lens and the anterior parts of the eye. The apparatus contains two channels that deliver light to the retina. The first channel illuminates the measuring field (1.9, 2.8 or 4.2 deg) on the retina. In this path, a rotating wheel (14 rev/sec) offers a sequence of 14 interference filters in the range 410–740 nm (bandpass 7 nm) to enable quasi-simultaneous measurement of reflectances across the visual spectrum. Interspaced are 6 stops to retrieve dark counts of the photomultiplier and (room-light) background level. The mean intensity over time was 1200 Td, ensuring that the bleaching of the visual pigment due to illumination of the measuring field was kept at a low level.

The second channel (30 deg) is used for bleaching. A Schott OG495 and a neutral density (ND) filter were used to limit the bleach intensity to a safe level of 5.8 log Td. For dark adaptation an ND filter was inserted which lowered the level to 200 Td. This level still enabled fixation at the cross-hair in the bleach channel.

Light reflected from the fundus in a detection field (1.6 deg) concentric to the illumination field was measured with a photomultiplier in photon count mode. Within the detection field the retina was assumed to be homogeneous. A microcomputer in the instrument accumulated (dark-corrected) counts for each interference filter and sent them, once a second, to a desktop computer for further processing.

Calibration

A surface painted with Eastman 6080 white was used to calibrate reflectance. The spectral reflectance of this paint was tested to be similar ($\pm 4\%$) to the spectral flatness of a $BaSO_4$ surface. Using the 4.2 deg illumination field, the reflectance measured at 220 mm from the pupil plane of the instrument was set at 1%, assuming a focal distance of the eye of 22 mm and Lambertian reflectance.

The instrument's stray-light for the different illumination fields was measured with a "black hole". This "black hole" consists of a polished black perspex plate, placed at a 45 deg angle in the pupil plane of the instrument. At this position there is a maximum separation between illumination and detecting beams. The minimal specular stray-light at the surface is further absorbed by the matt black anodized inner surface of an aluminum enclosure tube, that tightly fits around the exit lens to prevent roomlight entering the instrument. The reflectance of the "black hole" itself was estimated to be less then 0.001%. Maximum stray-light of the densitometer (0.03% of a white retina) was measured at the shortest wavelength (410 nm). The percentage reflectance $R(\lambda)$ from the eye, for each illumination field (illum), was calculated from the (instrument-corrected) counts measured from the eye and the (instrument-corrected) counts from the white surface as follows:

$$R(illum, \lambda) = \frac{N_{\text{meas}}(illum, \lambda) - N_{\text{instr}}(illum, \lambda)}{N_{\text{white}}(4.2\,\text{deg}, \lambda) - N_{\text{instr}}(4.2\,\text{deg}, \lambda)} \quad (1)$$

Protocol

Both the retinal angle of the reflected light and the bleach state of the visual pigments were varied, in order to test their influence on pathways of light through the receptor layer. All measurements were obtained from the fovea by setting the fixation target at the center of the illumination field. A bite-board and temple pads were used to maintain head position. A mydriatic was used to dilate the pupil. Reflection measurements to test directionality were performed with the instrument's entry and exit pupils aligned to the peak of the Stiles–Crawford (SC) function (van Blokland & van Norren, 1986). The position of the SC peak is slightly nasal in most subjects (about 1 mm in the pupil plane). A second pupil position 2.5 mm temporal to the SC peak and thus closer to the edge of the pupil was chosen to lower the light guided into the receptors. We shall refer to these two pupil positions in terms of retinal angle, calling the peak SC position "perpendicular" and the temporal position "oblique". The densitometer was aligned to the peak of the SC function by carefully monitoring both the measured counts and the retinal image, while making slight adjustments to the pupil position. The retinal image was optimized for brightness and contrast, thereby avoiding reflections from the cornea and lens. In most subjects perimacular reflections appear concentric when the entrance and exit pupils are at the SC peak. Photon counts were maximized for the medium and long wavelengths (>550 nm), while at the same time keeping the reflection for 410 nm below 0.05%. At 410 nm the retinal signal is very low, mainly due to the high density of the lens at this wavelength. Low counts at this wavelength are a good indication for the absence of corneal reflections. The interception of entrance or exit light by the pupil, as indicated by a sharp decrease in measured counts, was avoided.

The amount of visual pigment was controlled by the radiance of the bleach light. The decrease in bleach efficiency for the oblique pupil entry position compared to the perpendicular position was calculated as 0.3 log unit (Coble & Rushton, 1971). We used the Rushton equation (Wyszecki & Stiles, 1982) to calculate the unbleached fraction of visual pigment in the four conditions: perpendicular bleached, 0.03; perpendicular dark, 0.93; oblique bleached, 0.06; oblique dark, 0.97.

To obtain an adequate signal-to-noise ratio, the densitometer outputs were first averaged at 10 sec intervals. Twelve of the 10 sec averages were again averaged to give a final reflection data point (block of 2 min). The standard deviation was calculated from the twelve, 10 sec averages and mainly reflects photon noise and minor disturbances caused by short-term movements

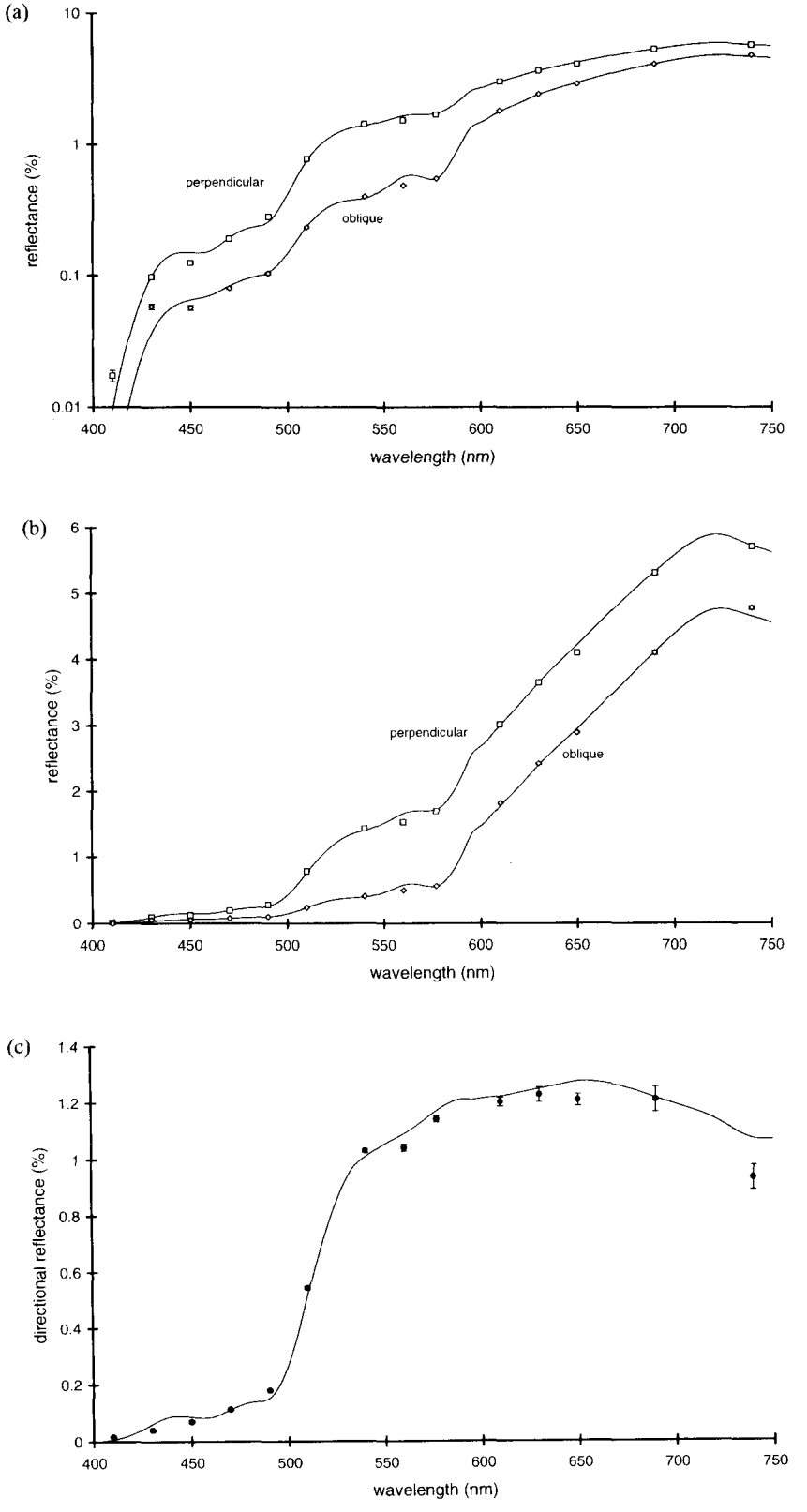

FIGURE 1. (a) Reflectance spectra of a bleached fovea for perpendicular and oblique measuring angles. Continuous lines are results from model fitting; points are data obtained from the first author (J.K.). In this and subsequent figures all data points and model curves below 0.01% were omitted as being not relevant. Illumination field size is 1.9 deg; detector field size 1.6 deg. Reflectance is referred to a white diffuse retina. (b) Identical data as in (a), but now plotted on a linear scale. (c) The directional reflectance, being the difference in reflectance between the model spectra and data points from (b). Although the model curve is a secondary result of the global fitting to the four primary spectra and not a direct fit to the data points in this figure, the fitting is still acceptable. At 540 nm and higher, the directional component is fairly constant. At the shorter wavelengths (below 540 nm), the double pass of lens and macular pigment reduces the magnitude of the difference. At the long wavelengths absorption by water is involved.

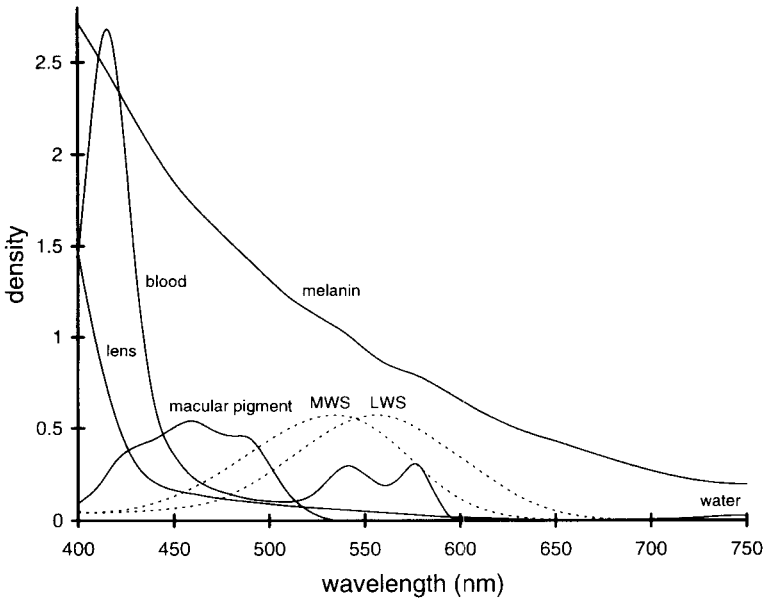

FIGURE 2. Absorption spectra of blood, melanin, macular pigment, the lens and water in the eye for a single pass. Mean results of model fitting are used to give representative densities for an average subject. For sources of the spectral shape see text. The thickness of the blood layer is 23 μm, with an oxygenation of 95%. Melanin density is 1.32 at 500 nm; macular pigment density is 0.54 at 460 nm; lens density at 420 nm is 0.54; water density is 0.025 at 740 nm (24 mm). Visual pigment densities are equal, 0.57 at the peak both for LWS and MWS cones, and are shown by the dotted lines.

of the subject. Alignment with the bleach light on took a few minutes. Data recording was then started with the bleach light on for an additional 2 min, to obtain an initial bleached spectrum. The dark period lasted at least 10 min, the last 2 min being used to obtain the dark-adapted spectrum. The spectrum obtained in the last 2 min of a second bleach period, lasting at least 5 min, was considered the (final) bleached spectrum. If the 560 nm point of the final bleached spectrum differed by more than 0.03 log unit from the initial bleach spectrum, the run was rejected. Each experimental run lasted 15–20 min for one alignment.

Subjects

All subjects were Caucasian and had normal color vision, as assessed from their Rayleigh Matches. Two experienced subjects with normal vision, the first two authors, took part in the pilot experiments. More extensive data were obtained for ten subjects, including the authors. The purpose of the experiment was explained and written informed consent was obtained.

EXPERIMENTAL RESULTS

Experiment 1: Directionality

Figure 1(a) shows spectra (for subject J.K.) measured in a bleached retina under "perpendicular" and "oblique" conditions (c.f. Methods). Continuous lines are fits from the model discussed later; symbols represent experimental data. The visual pigments were bleached away, and the 1.9 deg illumination field was used. Both spectra showed the following features. Reflectance was highest (about 5%) in the long wavelength part of the spectrum (above 600 nm). Melanin is virtually the only absorber in this spectral region (see Fig. 2 for the absorbers used in later analysis). Below 600 nm the sudden decline in reflectance was caused by absorption by blood. Reflectance decreased to a level equal to what we assume to be the reflectance from the outer segment layer. Reflectance between 510 and 430 nm was further reduced because of absorption by the macular pigment. At 430 and 410 nm reflectance decreased sharply due to lens absorption. As a consequence small residual reflections from the cornea had a relatively large influence on the data. Therefore, in this and subsequent figures all data points and model curves below 0.01% were omitted (as being not relevant). In the middle of the spectrum there was a marked difference between the two conditions, the reflection for light perpendicular to the retina being about three times higher than for oblique light. We attribute this completely to directional effects in the cone photoreceptors.

In Fig. 1(a) the spectra are plotted on a logarithmic scale, as is usual to account for the large dynamic range. However, an interesting aspect is overlooked this way. On a logarithmic scale the greatest difference between the spectra (showing in fact the greatest ratio) is seen around 500–550 nm. This is lost when the reflectance spectra are plotted on a linear scale [Fig. 1(b)]. Instead, there is little difference in reflectance for wavelengths higher than 540 nm. This difference in reflectance (in our opinion representing the directional reflectance from the receptors) gained when going from oblique to perpendicular angle, is plotted in Fig. 1(c). The steep increase in

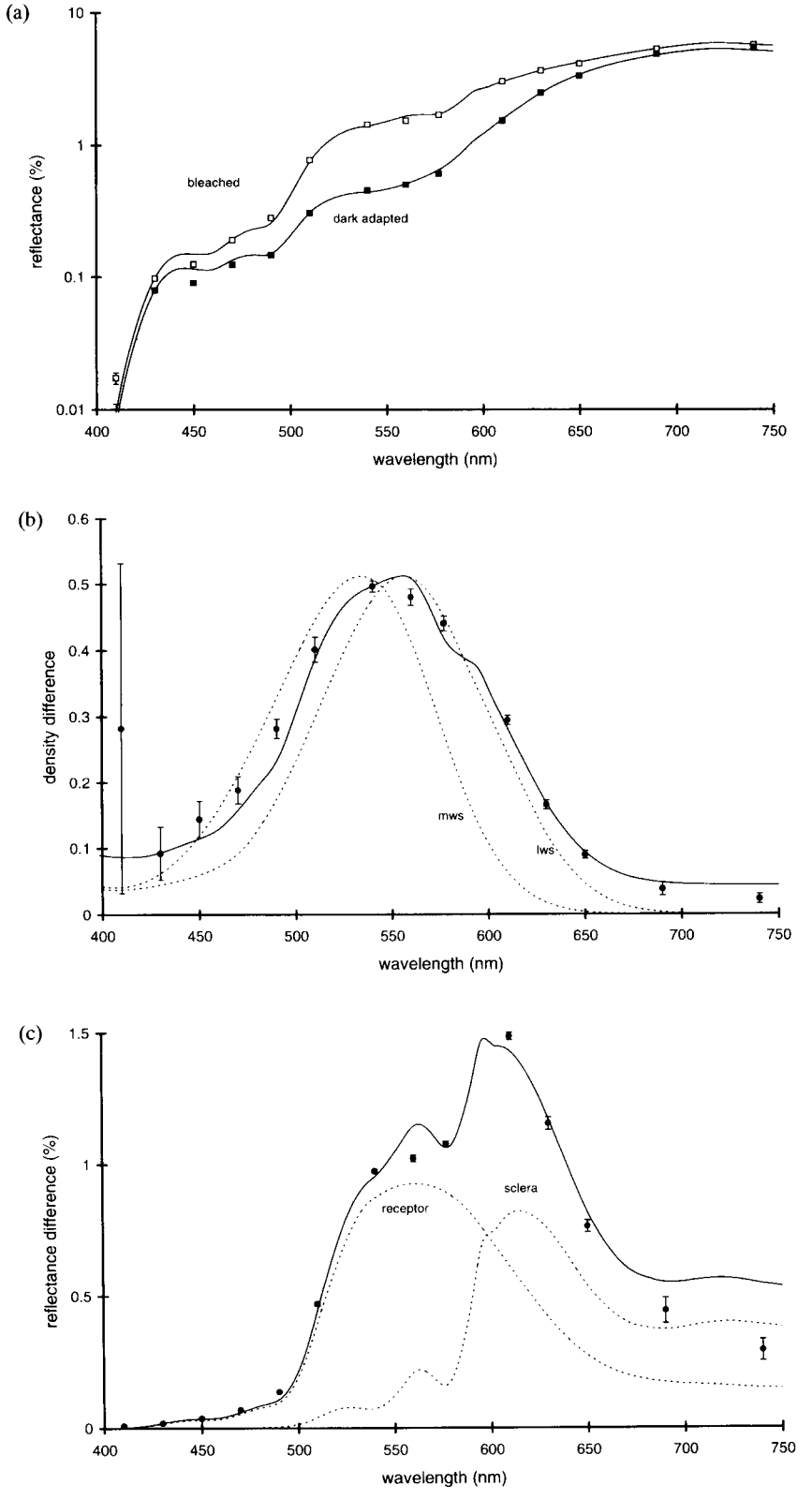

FIGURE 3. (a) Reflectance spectrum for the perpendicular measurement angle, measured for the bleached retina [copy of upper curve in Fig. 1(a)], together with the spectrum measured for the dark-adapted retina. Continuous lines are the results of the model fitting; points are experimental data. (b) Measured density difference spectrum (data points) and a model curve (continuous line), defined as the difference between the logarithmic scaled spectra in (a). Although the model curve is a secondary result of the global fitting to the four primary spectra and not a direct fit to the data points in this figure, the result is still acceptable. For comparison, dotted lines show visual pigment absorption curves (DeMarco *et al.*, 1992) for LWS and MWS cones. Their peak densities were set equal to the peak of the measured data. (c) Absolute reflectance difference between the spectra in (a) on a linear scale. This represents the light gained when a dark-adapted fovea is bleached. The continuous line is the model fit. Again this is a secondary result of the global fit to the four primary spectra. Dotted lines show the components from the model fit for light reflected at the receptor discs and the sclera.

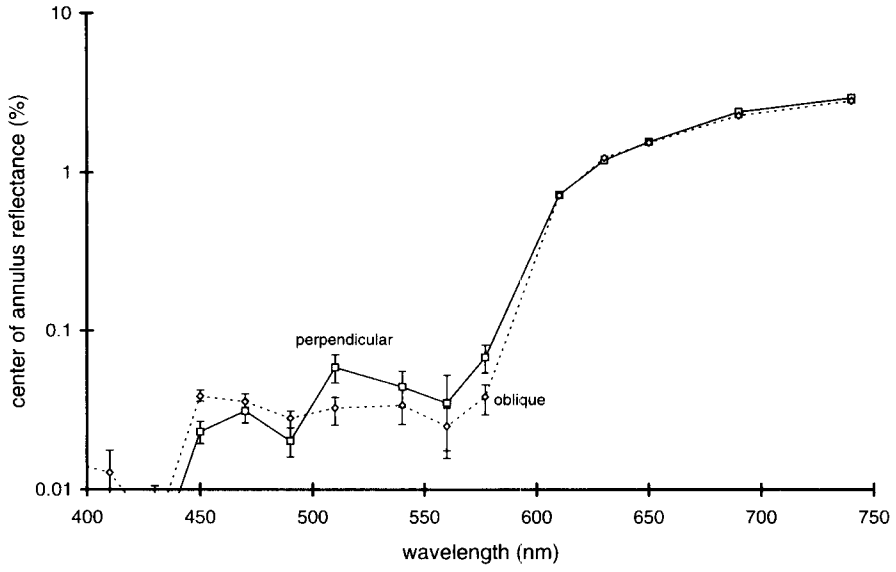

FIGURE 4. Reflectance spectra (subject J.K.) measured from the central 1.6 deg fovea, with an annulus with borders of 4.2 and 2.8 deg as illumination (see text). Shown are the perpendicular and oblique conditions measured in a bleached retina. Data points below 610 nm are noisy due to the subtraction of low values (see experiment 3). Lines in this figure are not based on model prediction, they just connect the data points for visibility. The data in this figure represent the spectral shape of the "deep" reflected light. The similarity between the two curves, especially at the long wavelengths, indicates the absence of directional effects in this deeper light.

absorption by blood at wavelengths below 610 nm is not, or at most to a very minor extent, seen in the directional spectrum, in particular when compared to the substantial influence of absorption by blood on the original reflection data shown in Fig. 1(a). The decline below 560 nm coincides with increasing absorption by the macular pigment and below 450 nm with absorption by the lens. As will be shown later, the decline at the longest wavelengths is largely due to absorption by water. This experiment suggests that the directional reflection from the receptors has a constant magnitude over a broad range of wavelengths and the spectral shape shown in Fig. 1(c) is only due to pre-receptor absorbers. This experiment supports the suggestion (c.f. Introduction) that the deeper, blood-rich layer reflects non-directional light.

Experiment 2: Varying visual pigment

The impact of the visual pigment on the foveal reflection is illustrated in Fig. 3(a). Two "perpendicular" spectra are presented, one for the bleached and one for the dark-adapted condition. The difference between these logarithmic plots is the well-known result of retinal densitometry [Fig. 3(b)]. This curve is traditionally ascribed to the double traverse of measuring light through the visual pigments. According to the simple model (c.f. Introduction), spectral aspects of posterior reflectors and anterior absorbers do not influence this type of result, and only the spectral density of the visual pigment is assumed to be relevant. For comparison, the absorption spectra of the long and medium wavelength-sensitive visual pigments (DeMarco *et al.*, 1992) are also shown. The model curve in this figure is a secondary result of the later described fit to the four original spectra and is not a result of a separate fit applied directly to the data points in this figure.

The absolute linear difference between the perpendicular spectra from Fig. 3(a) is plotted in Fig. 3(c). This difference in reflectance reveals details that go unnoticed in the logarithmic difference of Fig. 3(a) (that shows in fact ratios). These data represent the absolute reflectance gained when going from the dark-adapted to the bleached state. The maximum appears at 610 nm, instead of 550 nm as seen in Fig. 3(b). There is an abrupt decrease at wavelengths below 610 nm, indicative of absorption by blood. The retinal vascular system is unlikely to have a great influence as it did not affect the results of experiment 1, and there are no indications of such absorption in the psychophysical spectral sensitivity curves of the fovea. This experiment proves the existence of a pathway of light that traverses the photoreceptors and also the deeper, blood-rich layers. To illustrate this, the results of the two underlying components (sclera and receptor discs) obtained by the model fitting are also shown [dotted lines in Fig. 3(c)]. Again, the model curves in this figure are a secondary result of the later described global fitting.

Experiment 3: Directionality of light from deeper layers

A more complex experiment provided additional evidence for the non-directionality of the light reflected by the deeper layers. When illumination and detection fields do not overlap in the retinal plane, there is no reflection from receptor and superficial retinal layers and only laterally diffused light from the deeper layers

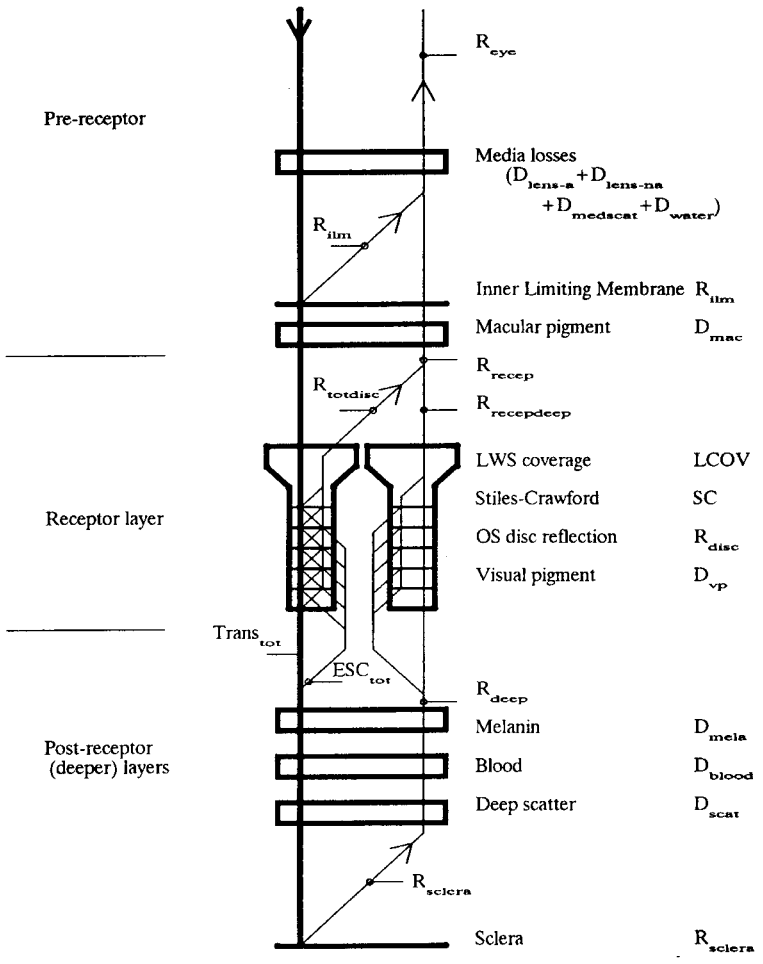

FIGURE 5. Model of optical reflectance of the fovea, with pathways through the receptor layer and reflections from the ILM, the receptor discs and the sclera. Reflectors are indicated by horizontal lines. Absorbing pigments are drawn as horizontal boxes. Cones are depicted as funnel-shaped objects. In the dark-adapted condition the cones are filled with visual pigment. Light enters the eye from the top, as indicated by the downward pointing arrow. Upward pointing arrows represent light detected by the instrument, emerging from the eye after reflection from the different layers. Secondary reflections are assumed to be lost elsewhere. Only the reflection from the cone receptor discs is directional. For a complete description of the model see Model section.

remains. This was achieved by subtracting the spectrum measured with an illumination field of 4.2 deg from the spectrum measured with an illumination field of 2.8 deg. In this way light entering in an annulus with borders at 4.2 and 2.8 deg and emerging from the retina from the central detection area of 1.6 deg diameter is obtained. Measurements in the bleached condition showed that very little light emerges at wavelengths below 610 nm (Fig. 4, subject J.K.). It is difficult to make an absolute comparison with the other spectra because more light entered the eye (reflectance is only clearly defined for local light). This result proves that the light has indeed traveled through the deeper layers and that there was strong absorption by blood and melanin. There was virtually no difference in reflection at the long wavelengths when the results for the perpendicular and oblique conditions were compared. For shorter wavelengths, the amplitude of the difference was low and even negative due to noise, because of the subtraction of almost identical data from the original measurements with 4.2 and 2.8 deg illumination field. From this experiment we can conclude that the light reflected from the deeper layers is non-directional, even after passing the receptor layer with strong directional properties.

MODEL

General introduction

Our starting point was the model developed by van Norren & Tiemeijer (1986), with some of the modifications suggested by Delori & Pflibsen (1989). Our model includes the receptor layer, which was ignored by van Norren & Tiemeijer (1986) and Delori & Pflibsen (1989). The model (Fig. 5) is divided into three main parts, the pre-receptor (mainly eye media), the receptor and the post-receptor part (all deeper layers). Light entering the eye is represented by a vertical thick line (left) with a downward pointing arrow and light emerging from the eye is represented by a vertical thin line (right) with an upward pointing arrow. In Fig. 5 the absorbing layers are

TABLE 1. Spectral data from the literature that were used for the model fitting; for sources see text

Wave	Lens-a	Lens-na	Water	Mac	MWS	LWS	Mela	Blood	Sclera
410	0.4388	0.66473	0.00020	0.1642	0.0806	0.0730	0.7695	0.10793	0.999
430	0.3240	0.10332	0.00018	0.3643	0.1206	0.0875	0.6600	0.06089	0.948
450	0.2537	0.00453	0.00018	0.4596	0.2309	0.1164	0.5604	0.01564	0.900
470	0.2007	0.0	0.00018	0.4467	0.4112	0.1796	0.4900	0.00764	0.854
490	0.1607	0.0	0.00022	0.4037	0.6423	0.3421	0.4298	0.00518	0.810
510	0.1267	0.0	0.00039	0.1326	0.8694	0.5828	0.3705	0.00448	0.769
540	0.0920	0.0	0.00059	0.0	0.9902	0.9310	0.3094	0.01296	0.711
560	0.0688	0.0	0.00075	0.0	0.8076	0.9958	0.2605	0.00834	0.675
577	0.0492	0.0	0.00103	0.0	0.5330	0.8803	0.2395	0.01350	0.646
610	0.0232	0.0	0.00302	0.0	0.1212	0.4733	0.1801	0.00027	0.592
630	0.0112	0.0	0.00334	0.0	0.0346	0.2356	0.1501	0.00017	0.562
650	7.4E-4	0.0	0.00366	0.0	8.27E-3	0.0902	0.1299	0.00012	0.534
690	0.0	0.0	0.00525	0.0	4.30E-4	0.0068	0.0900	0.00009	0.481
740	0.0	0.0	0.02458	0.0	1.52E-5	2.63E-4	0.0600	0.00012	0.422
	420 nm	420 nm		460 nm			500 nm		
	0.3724	0.3080		0.495			0.40		

"Wave" is the wavelength, "Lens-a" is the aging part of lens density, "Lens-na" is the non-aging part of lens density, "Water" is the density of 24 mm water, "Mac" is the density of the macular pigment, "MWS" and "LWS" are normalized (energy) sensitivities of the medium and long wavelength sensitive visual pigments, "Mela" is melanin density, "Blood" is the density of 1μm of 95% oxygenated blood, "Sclera" is the reflectance of the sclera. Data were interpolated by a polynomal to 1 nm resolution and convoluted with the 7 nm bandwidth of the interference filters. The 740 nm MWS and LWS data were extrapolated by fitting a straight line through the last original data points. Where applicable, at the bottom of the column, the wavelength and value of normalization are given.

represented as horizontal boxes. Spectral data for these layers were convoluted with the 7 nm bandwidth of the filters used in the measurements (Table 1). The spectral data with densities for an average subject are shown in Fig. 2. Single horizontal lines in Fig. 5 represent reflecting layers. The receptors are depicted as vertical funnel-shaped objects. Reflecting layers are assumed to be spectrally neutral, as is the case for Fresnel refraction on layer boundaries with a small difference in the refractive index. An exception is the reflectance of the sclera, that was assumed to decrease slightly in the long wavelength part of the spectrum (see the next section). Secondary reflections at the back of reflecting layers (when going upward in the drawing) do not contribute to the measured signal. The model is discussed in detail below. We start at the scleral side because the reflectances of posterior layers are components in the calculation of anterior reflectances. Only those parameters that are allowed to vary in the process of fitting the experimental data are numbered.

Post-receptor (deeper) layers

We modeled the deeper layers in a very simplified way similar to that of van Norren & Tiemeijer (1986), with absorption by melanin and blood and reflection from the sclera. Delori & Pflibsen (1989) presented a more complex model of the deeper layers. They used fixed values for epithelial melanin and blood in the choriocapillaris and added a more complex reflection in the choroid, using Kubelka–Munk scattering with a fixed tissue scatter term. This resulted in an estimate of the density of choroidal melanin and the thickness of the blood layer. The numbers for blood and melanin are higher (and more realistic in an physiological sense) than the van Norren and Tiemeijer data, but this is at the expense of the three extra parameters. In addition, the results are (1) quite sensitive to the tissue scattering term, which was fixed at a very weak optimum, and (2) the Kubelka–Munk scatter model is only one-dimensional and ignores sideward scattering. We think that a more complex three-dimensional model, including reflection from Bruch's membrane, and parallel and serial pathways through blood, melanin and tissue, is needed to obtain more precise parameter estimates. As our main interest was not in the deeper layers, but in the behavior of the receptor layer, we did not employ Kubelka–Munk modeling. We only needed a short and simple characterization of the reflection from the deeper layers. By ignoring the details of choroidal parallel pathways and scatter, the values for blood layer thickness and melanin density are underestimated.

The reflectance of the sclera was assumed to decrease in the long wavelength part of the spectrum (Delori & Pflibsen, 1989). It is described by a fixed parameter:

$$R_{\text{sclera}}(\lambda) = 0.5 \cdot \exp(-0.00261(\lambda - 675)). \quad (2)$$

Parameter 1. Density of deep scatter losses (D_{dscat})

To allow for spectrally neutral losses at the deeper layers (for instance light scattering out of the detection field), a free parameter D_{dscat} was added (Delori & Pflibsen, 1989).

Parameter 2. Thickness of bloodlayer (Th_{blood})

We assumed the oxygenated fraction to be 0.95 (Delori & Pflibsen, 1989). Blood absorption data (both HB and HBO_2) were taken from van Assendelft (1970). The free parameter, Th_{blood}, represents the thickness of an equivalent layer of blood in micrometers. This value was converted to the optical density of blood $D_{\text{blood}}(\lambda)$ by using the extinction values from Assendelft (see Table 1

for densities of 1 μm blood). The concentration used was 150 mg/l and the molecular weight was 16.1 mg/mmol.

Parameter 3. Density of melanin (D_{mela})

The shape of the melanin absorption curve was taken from Gabel *et al.* (1978) with the density at 500 nm as the free parameter D_{mela}.

Calculating reflectance of the deeper layers

The formula for sclera reflectance gives unrealistic values near 100% reflectance for the shorter wavelengths (Table 1). Fortunately, these high values are not important, because the high absorption of blood and melanin in this spectral region virtually eliminates any influence of deeper reflected light compared to the influence of reflection from the photoreceptor discs.

The reflectance of the deeper layers is calculated as:

$$R_{\text{deep}}(\lambda) = R_{\text{sclera}}(\lambda) \cdot 10^{-2}(D_{\text{mela}}(\lambda) + D_{\text{blood}}(\lambda) + D_{\text{dscat}}) \quad (3)$$

Receptor layer

The receptors in this layer are depicted by the vertical funneling elements in Fig. 5 (two cones are shown rather than one, to avoid crowding of the entering and emerging light paths). Because of their small dimensions, receptors can be considered as optical waveguide antennas (Snyder & Pask, 1973). Antennas are reciprocal, the lobes that describe the directional reception also apply when they radiate. Antennas usually have a pronounced forward lobe, making reception most effective for a perpendicular angle. At oblique angles, less energy is captured and more escapes to the surroundings. With knowledge of the directional forward lobe, the so-called antenna gain and the effective capture area can be determined (Jessop, 1971). The antenna gain is defined as the ratio of the area of a hemisphere and the weighted cross-sectional area of the lobe at the hemisphere. The capture area is defined as the effective reception area and may be larger than the physical dimensions of the antenna. The antenna gain is high and the capture area is large when the directionality of the receiving pattern is high (see Appendix). If the foveal receptors are considered as antennae, the capture area for perpendicular light is calculated to be larger than the area covered by the receptor itself. This means that we can assume that all the light is captured by the inner segments of the receptor and then travels onto the outer segments. In conclusion, for our detection field we assume light not to enter the receptor interspaces in this perpendicular condition.

For oblique angles, light has to enter the interspaces between the outer segments in order to explain the decreasing psychophysical Stiles–Crawford efficiency. Psychophysical experiments (King-Smith, 1973b; Burns & Elsner, 1993) show an apparent decrease in the thickness of the visual pigment layer at oblique angles. This apparent decrease also narrows the absorption spectra of the visual pigment. Considering the case where light already escapes at the inner segment level instead of escaping along the outer segment, then the fraction of light still guided through the outer segment always encounters the full length of the visual pigment layer. In that case there would be no spectral narrowing of absorption spectra. We therefore assume, as proposed earlier by Walraven & Bouman (1960) that, for oblique angles, light gradually escapes along the outer segment into the receptor interspaces. This results in an exponential decay of guided light within the outer segment.

Parameter 4. Stiles–Crawford (SC) effect

To quantify the captured light as a function of retinal angle, we implemented a Stiles–Crawford (SC) parameter fixed at 1 for the perpendicular condition and between 0 and 1 for the oblique condition. We defined parameter SC as the transmission of the total outer segment due to the apparent absorption of the escaping light. The escaping fraction is then 1 − SC. For the uniformity of later calculations we converted the free parameter SC to the density of the apparent absorption; D_{esc} defined as:

$$D_{\text{esc}} = -\log(SC). \quad (4)$$

Parameter 5. Receptor disc reflectance (R_{disc})

For an array of receptors with overlapping capture areas (see Appendix) and reflection at the outer segment discs, the apparent reflectance for the whole array equals the apparent reflectance of a single outer segment, although the latter has a smaller diameter. At an oblique angle, light escaping from the outer segment lowers the apparent disc reflectance, as only the light remaining in the outer segment "sees" the discs. This is the basis for directional reflection according to our view (c.f. Introduction).

The free parameter, R_{disc}, is taken to represent the total reflectance of the discs in the absence of other factors. Again, we converted this reflectance for the uniformity of later calculations into an apparent density of a single pass through the outer segment. D_{disc} is calculated as:

$$D_{\text{disc}} = -\log(1 - R_{\text{disc}}). \quad (5)$$

Parameter 6. LWS cone coverage fraction (LCOV)

We distinguish between medium (MWS) and long (LWS) wavelength sensitive cones. Short wavelength sensitive cones are so sparse that they can be neglected (Curcio *et al.*, 1991). The ratio of the numbers of long and medium sensitive cones is represented by their average coverage fractions, LCOV and MCOV. We argued before that, based on the capture area of the receptors, no light enters directly into the interspaces. We therefore took the sum of LCOV and MCOV as unity.

Parameter 7. Density of the visual pigment (D_{vp})

The peak visual pigment density, D_{vp}, was assumed to be equal for LWS and MWS cones [short wavelength sensitive (SWS) cones were ignored] and was a free parameter. The spectral shapes were taken from DeMarco

et al. (1992). In Fig. 5 each cone can contain only one visual pigment. The density as a function of wavelength of LWS visual pigment, $D_{lws}(\lambda)$, is obtained by multiplying the normalized LWS density spectrum and D_{vp}. Substituting MWS for LWS gives $D_{mws}(\lambda)$ for the MWS visual pigment.

Calculating the reflectance of the receptor layer

The reflectance of the receptor layer in our model consists of two components: (1) the direct reflectance from the discs; and (2) the reflectance of light which has traversed the receptors (either the full outer segment, or partly when escaping along the outer segment) and the deeper layers.

Reflectance of the discs. Macroscopically we view the reflection from the individual discs as a homogeneously distributed reflectance over the full depth of the outer segment. This distributed reflection (seen from the inner segment) is influenced by losses due to (1) the absorption of visual pigment, (2) light escaping along the outer segment for oblique angle and (3) light reflected from the discs. We already assumed that the losses (2) and (3) act as homogeneous distributed optical filters, and we used a similar assumption for visual pigment. Consequently, measured light from discs near the inner segment has a higher amplitude than that of measured light from discs near the end of the outer segment. The pathlengths, from zero to the full length of the outer segment through the homogeneous optical filter, act as a graded (wedge shaped) filter. The resulting transmission from such a filter of maximum density D is described by:

$$T_{graded} = \frac{1 - 10^{-D}}{D \cdot \ln(10)} \tag{6}$$

The density of visual pigment and densities due to escaped light and disc reflection losses are substituted for D in equation (6). Pathways for escaped light run from the inner segment to the position of escape along the outer segment and back. So do the pathways for visual pigment (going in and out the receptor). We ignored secondary reflection losses at the back of the discs, permissible if the reflectance is in the order of a few percent. Multiplication by a normalizing factor $D_{disc} \cdot \ln(10)$ is needed to arrive at the definition for reflectance R_{disc}, when D_{lws} and D_{esc} are zero. We then find for the total reflectance of the discs of LWS cones:

$$R_{lwsdisc}(\lambda) = \frac{D_{disc} \cdot (1 - 10^{-(2D_{lws}(\lambda) + 2D_{esc} + D_{disc})})}{2D_{lws}(\lambda) + 2D_{esc} + D_{disc}} \tag{7}$$

and a similar expression for the MWS cones $R_{mwsdisc}(\lambda)$.

The total reflectance from the discs of both LWS and MWS cones is:

$$R_{totdisc}(\lambda) = LCOV \cdot R_{lwsdisc}(\lambda) + MCOV \cdot R_{mwsdisc}(\lambda) \tag{8}$$

Light transmitted through the outer segment. The transmission of the total length of the LWS cone outer segment, $Trans_{lws}$ is simply determined by the addition of the underlying densities as:

$$Trans_{lws}(\lambda) = 10 - (D_{lws}(\lambda) + D_{esc} + D_{disc}). \tag{9}$$

and similarly for the MWS cones $Trans_{mws}(\lambda)$.
The total transmission of LWS and MWS cones is:

$$Trans_{tot}(\lambda) = LCOV \cdot Trans_{lws}(\lambda) + MCOV \cdot Trans_{mws}(\lambda) \tag{10}$$

Light escaping along the outer segment. For the escaped light we have to account [in a similar way as for the calculation of reflectance of the discs in equation (7)] for the graded density of visual pigment, the density due to light already escaped, and the density due to light already reflected from the discs. Only the pathways from the first disc (inner segment side) to the position along the outer segment where the light escapes into the interspace have to be considered. Multiplication by a normalizing factor $D_{esc} \cdot \ln(10)$ is needed to arrive at the definition for the escaped fraction in the absence of losses from visual pigment and disc reflection. For the LWS cones the escaped fraction is:

$$ESC_{lws}(\lambda) = \frac{D_{esc} \cdot (1 - 10^{-(D_{lws}(\lambda) + D_{esc} + D_{disc})})}{D_{lws}(\lambda) + D_{esc} + D_{disc}} \tag{11}$$

and similarly for the MWS cones $ESC_{mws}(\lambda)$.
For the total escaped light fraction of LWS and MWS cones we find:

$$ESC_{tot}(\lambda) = LCOV \cdot ESC_{lws}(\lambda) + MCOV \cdot ESC_{mws}(\lambda). \tag{12}$$

Reflectance of the receptor layer including light paths traversing the deeper layers. Light entering the deeper layers consists of a fraction that has been transmitted through the outer segments and a fraction that has escaped from the outer segments. The reflectance for pathways traversing the deeper layers and the receptor layer is:

$$R_{recepdeep}(\lambda) = (Trans_{tot}(\lambda) + ESC_{tot}(\lambda))^2 \cdot R_{deep}(\lambda) \tag{13}$$

The total reflectance at the level of the receptor layer is given by:

$$R_{recep}(\lambda) = R_{totdisc}(\lambda) + R_{recepdeep}(\lambda) \tag{14}$$

Pre-receptor part

It is assumed that pre-receptor reflection and transmission is non-directional, ignoring minor inhomogeneities in lens absorption over the pupil (Vos & van Os, 1975). Specular reflections from the eye media are avoided in our fundus reflectance measurements.

Parameter 8. Density of macular pigment (D_{mac})

Spectral absorbance by the macular pigment was taken from DeMarco *et al.* (1992). As the spatial distribution is not flat, the free parameter D_{mac} represents the average density at 460 nm over our measuring field (1.6 deg).

Parameter 9. Reflectance of the inner limiting membrane (R_{ilm})

The free parameter ILM reflectance (R_{ilm}) is assumed spectrally neutral. We also assume non-directional diffuse reflection, as in our measurements, except for the tiny reflex that was sometimes present at the very center of the fovea, specular reflection was not visible. Minor backscatter in the vitreous cannot be distinguished from the ILM reflectance and is included in this parameter.

Parameter 10. Lens aging part ($D_{lens\text{-}a}$)

The density of the media consists of four components, the fixed spectral density of the non-aging lens part ($D_{\text{lens-na}}$), the spectral density of the age dependent lens part ($D_{\text{lens-a}}$), which we allowed to vary, the fixed density of the spectrally neutral scatter losses (D_{medscat}), and the fixed spectral density of 24 mm of water (D_{water}), representing the vitreous. The parameter values for $D_{\text{lens-a}}$ and $D_{\text{lens-na}}$ are the densities at 420 nm. Spectral data were from the van Norren & Vos (1974) standard observer with the aging algorithm from Pokorny *et al.* (1987). Since our measurements were not restricted to the center of the pupil, the 0.86 correction term for large pupils was applied to $D_{\text{lens-a}}$ and $D_{\text{lens-na}}$. The term D_{medscat} represents scatter losses in the media (mainly lens, but also some loss due to the corneal reflectance). Delori & Pflibsen (1989) suggested a fixed value of 0.1 for this parameter, D_{medscat}. We used 0.15, the value provided by van Norren & Vos (1974) for non-spectacle wearers and an additional 0.05 for spectacle wearers. Absorption by the vitreous, taken to be that of pure water (Smith & Baker, 1981), was only significant at the longest wavelengths (0.025 at 740 nm).

Calculating the reflectance at the level of the cornea

Finally, we have to account for reflection and absorption by the media in order to determine the reflectance of the whole eye.

$$R_{\text{eye}}(\lambda) = 10^{-2(D_{\text{lens-na}}(\lambda)+D_{\text{lens-a}}(\lambda)+D_{\text{medscat}}+D_{\text{water}}(\lambda))} \cdot (R_{\text{ilm}} + (1-R_{\text{ilm}})^2 \cdot 10^{-2D_{\text{mac}}(\lambda)} \cdot R_{\text{recep}}(\lambda)) \quad (15)$$

FITTING EXPERIMENTAL DATA

Fitting procedure

Parallel channels in the model call for a fitting algorithm capable of handling non-linear parameters. We therefore applied the Marquardt–Levenberg fitting algorithm (Press *et al.*, 1989). The model has 10 free parameters (3 pre-receptor, 4 receptor layer and 3 post-receptor). To allow optimal fits, we allowed an extra correction density D_{ct}, giving 11 free parameters (see below). The freedom of fitting was limited because in the four spectra, measured for perpendicular and oblique retinal angle and both in fully bleached and dark-adapted conditions, 48 data points had to be fitted simultaneously. From the total of 11 free parameters, only three parameters were allowed to vary between the four spectra, namely, the Stiles–Crawford (SC) parameter, the amount of visual pigment density D_{vp} and the correction term D_{ct}. D_{vp} was set at zero for the bleached condition. SC equalled 1 for the perpendicular condition (no leakage) and had a positive value lower than 1 for the oblique condition. The free correction parameter, D_{ct}, was required only in the perpendicular condition. Most spectral absorbers we used tend to become zero at the long wavelengths; this limits the degrees of freedom we have for the fitting process. This was in particular a problem when small reflectance differences occurred between dark and bleached spectra that could not be fully explained by the low visual pigment absorption at the long wavelengths. The visual pigment parameter, being the only free parameter allowed for fitting the difference here, was then strongly influenced. The differences are considered to originate from small alignment disturbances between runs, from small changes in corneal reflection caused by suppression of the blink reaction during long periods of fixation, or from yet unknown processes. D_{ct} (either positive or negative) was therefore added to the media scatter term, D_{medscat}, in the perpendicular, dark-adapted condition.

The measured data for 410 and 430 nm were excluded from the fitting process, because these low reflection values were liable to small, and in some subjects due to changes in head fixation, variable amounts of back-scattered light from the cornea or lens. The data are included in the spectral plots, however, for comparison with the model results (see also experimental results).

The standard deviations (see Protocol) were used for weighting the data during the fitting process and are shown as error bars in the spectral plots of Figs 1 and 3. Note that these errors bars are minimum estimates, mainly expressing photon noise; errors due to long-term effects, for instance shifts in alignment between blocks, are not included. This is one reason for the model curves missing some data points. Another reason is that model curves as in Figs 1(c), 3(b) and (c) are not the result of separate fits to the data points in those figures, but secondary results from only one global fit to the four primary spectra. The reflectance data averaged over the group of ten subjects, together with the standard deviation for the group and the mean of the relative error in each subject, are shown in Table 2. The standard deviation for the group shows the inter-individual differences. The average of the relative errors, calculated from single measurement standard deviations, represents the average stability of a measurement. The parameters obtained from fitting the data for the ten subjects are shown in Table 3.

Results from the fitting process

The parameters obtained after the fitting process are now shortly discussed and compared with data found in the literature.

Deeper layers. Note that we simplified the model for the deeper layers. Parameters for blood and melanin are

TABLE 2. Mean spectral reflectance data for the ten subjects in four conditions

Wave (nm)	Perpendicular-bleached	Perpendicular-dark	Oblique-bleached	Oblique-dark
410	0.027 0.496 (0.216)	0.021 0.590 (0.334)	0.019 0.656 (0.809)	0.023 0.538 (0.244)
430	0.097 0.344 (0.075)	0.081 0.313 (0.077)	0.067 0.353 (0.097)	0.066 0.371 (0.127)
450	0.118 0.364 (0.050)	0.091 0.333 (0.050)	0.078 0.337 (0.074)	0.081 0.414 (0.069)
470	0.170 0.350 (0.040)	0.122 0.295 (0.037)	0.099 0.270 (0.048)	0.100 0.323 (0.056)
490	0.219 0.365 (0.033)	0.140 0.277 (0.039)	0.114 0.265 (0.051)	0.108 0.297 (0.052)
510	0.645 0.312 (0.023)	0.289 0.211 (0.034)	0.249 0.219 (0.041)	0.202 0.213 (0.045)
540	1.230 0.275 (0.016)	0.451 0.185 (0.023)	0.443 0.194 (0.024)	0.318 0.200 (0.031)
560	1.334 0.259 (0.016)	0.489 0.186 (0.025)	0.509 0.195 (0.024)	0.357 0.203 (0.031)
577	1.413 0.243 (0.015)	0.586 0.199 (0.019)	0.568 0.170 (0.020)	0.414 0.206 (0.024)
610	2.073 0.240 (0.012)	1.196 0.203 (0.016)	1.198 0.264 (0.017)	0.960 0.291 (0.019)
630	2.386 0.254 (0.012)	1.748 0.226 (0.014)	1.533 0.277 (0.016)	1.342 0.296 (0.015)
650	2.715 0.242 (0.012)	2.277 0.233 (0.011)	1.843 0.282 (0.015)	1.728 0.308 (0.013)
690	3.461 0.253 (0.014)	3.270 0.248 (0.014)	2.639 0.274 (0.018)	2.574 0.294 (0.017)
740	3.926 0.229 (0.014)	3.793 0.235 (0.012)	3.202 0.251 (0.015)	3.118 0.262 (0.014)

Data are percentages referred to a white Lambertian reflector, followed by the relative standard deviation. The relative standard deviation expresses mainly the intra-individual differences in reflectance. The average of individual relative errors is given in parentheses, as an indication of the relative error in one subject. This is mainly the result of photon noise and small movements of the subjects.

TABLE 3. Free and fixed parameters used in the model

Free parameter	Abbreviation	Method 1 mean,	sd,	range	Method 2 mean,	sd
Deep scatter loss	D_{dscat}	0.23	0.06	0.14–0.30	0.225	0.006
Blood layer (μm)	Th_{blood}	22.7	16.9	7.3–63.2	17.0	4.5
Melanin density	D_{mela}	1.32	0.23	0.98–1.68	1.274	0.028
Stiles–Crawford eff.	SC	0.21	0.11	0.07–0.41	0.193	0.022
OS disc reflectance (%)	R_{disc}	2.75	0.73	1.64–3.80	2.773	0.095
LWS cone coverage	LCOV	0.56	0.11	0.41–0.71	0.525	0.048
Visual pigment dens.	D_{vp}	0.57	0.11	0.41–0.80	0.587	0.026
Macular pigment dens.	D_{mac}	0.54	0.12	0.42–0.83	0.525	0.025
ILM reflectance (%)	R_{ilm}	0.26	0.09	0.12–0.44	0.260	0.024
Lens dens.	$D_{lens\text{-}a+lens\text{-}na}$	0.54	0.11	0.42–0.83	0.533	0.030
Media correction dens.	D_{ct}	0.018	0.009	0.003–0.036	0.0194	0.0028

The free parameter results are for a group of ten subjects. Two methods were used to calculate the averages. In the first method the spectral data from each individual were fitted, and the resulting parameters were averaged to give a group mean and standard deviation. The column 'range' gives the lowest to highest result of the fits. In the second method all corresponding spectra of the ten subjects were averaged to give data for an 'average subject' (Table 2), and subsequently fitted, resulting in a second mean and standard deviation for the 'average subject'. For lens density the results are the sum of the free lens aging parameter and the fixed lens non-aging parameter.

Fixed parameters:

Density of media scatter losses	$D_{medscat}$	0.15 (+0.05)
Density of non aging lens part	$D_{lens\text{-}na}$	0.31 at 420 nm
Density of 24 mm water	D_{water}	0.025 at 740 nm
Reflectance of the sclera	R_{sclera}	0.5 at 675 nm

therefore not necessarily comparable with physiological data (c.f. "Post-receptor (deeper) layers" section).

Parameter 1. Density of deep scatter losses

The deep scatter loss D_{dscat} (0.23), was higher than in the model of Delori & Pflibsen (1989) who found 0.1. This is because we used smaller fields. Delori and Pflibsen found reflectance in the long wavelength part of the spectrum, stemming mainly from deeper layers, to be higher than 10% for lightly pigmented subjects. This is only partly explained by the large (5 deg) illumination field they used. Van Norren & Tiemeijer (1986) did not use a D_{dscat} term, but allowed the sclera reflectance to change. Converted to the density of deep scatter losses and corrected for not having implemented media scatter losses, we found a density of 0.17.

Parameter 2. Thickness of blood layer

The thickness of the equivalent blood layer, Th_{blood}, was 23 μm. The mean value from van Norren & Tiemeijer (1986) is given as a density of 0.18 at 500 nm, corresponding to a thickness of 37 μm. Delori & Pflibsen (1989) obtained higher values (60 to 304, average 168 μm) when assuming Kubelka–Munk scattering in the choroidal space, but at the expense of introducing several parameters (c.f. Model section).

Parameter 3. Density of melanin

The density of melanin (1.32 at 500 nm) is mainly determined by the fit to wavelengths above 600 nm. At shorter wavelengths absorption by blood dominates. In addition, at the foveal site, our model shows that the reflection in the receptor layer strongly masks the reflection from deeper layers at wavelengths less than 570 nm. Melanin densities ranged from 0.98 to 1.68. This is in the lower end of the range found by Delori & Pflibsen (1989) (0.79–8.5). Van Norren & Tiemeyer (1986) reported a value of 0.98.

Receptor layer

Parameter 4. Stiles–Crawford factor

The Stiles–Crawford parameter, SC, depends on the setting of the retinal angles (adjustment). In the present context SC as such is not important but is needed only to determine the other parameters. The maximum value of 0.41 ensures that the fitting process can successfully discriminate the directional cone reflection from the non-directional reflection of the pre-receptor and the deeper layers. Note that our definition of SC was slightly different from the psychophysical convention, where it is a measure of light absorbed by visual pigment.

Parameter 5. Receptor disc reflectance

The combined reflectance from the discs over the full length of the outer segment (2.75%) can best be compared with the reflectance at the RPE assumed in the models of van Norren & Tiemeijer (1986) (1.18%) and Delori & Pflibsen (1989) (2.3%). The design of the entry and exit pupils of the apparatus influences the directional reflection. If van Norren & Tiemeijer (1986) had used media scatter in their model, their value converts to 2.36% (correction with twice 0.15 D).

Parameter 6. LWS cone coverage fraction

The coverage fraction of the LWS cones (0.56) is often expressed as the ratio of LWS to MWS cones. Converted to LWS coverage fraction, values of about 0.66 are reported (Vos & Walraven, 1970; Cicerone & Nerger, 1989; Kraft *et al.*, 1990).

Parameter 7. Density of the visual pigment

The visual pigment densities we calculated (0.57 for single traverse) are comparable with psychophysical results. In our calculations, we did not take into consideration whether the visual pigment was fully bleached or fully dark-adapted (see Protocol), so the value D_{vp} is a low estimate. The final result could be about 10% higher (0.63) if the Rushton equation is valid (see Protocol). Visual pigment densities decrease with field size. Smith & Pokorny (1973) found 0.3 for the MWS cone and 0.4 for the LWS cone, using a 2.5 deg test field. Miller (1972) reported 0.5–0.6 for LWS and 0.4–0.5 for MSW cones (1.6 deg test field). Burns & Elsner (1993) reported 0.3 for the MWS cone and 0.5 for the LWS cone, using 2 deg fields. Pokorny & Smith (1976) presented a formula to calculate the densities in relation to field size. For our 1.6 deg field, this would result in 0.52 for LWS and 0.42 for MWS cones. Walraven & Bouman (1960) reported 0.7, based on changes in self-screening of the visual pigments due to changes in Stiles–Crawford effect (2 deg field).

Pre-receptor part

Parameter 8. Density of macular pigment

The density of macular pigment (0.54 at 460 nm) differs substantially between subjects and also decreases with increasing field size. Bone *et al.* (1992) found 0.57 for a spot size of 1.6 deg (identical to our detection field size). Delori & Pflibsen (1989) used larger fields (illumination 5 deg, detection 1.2–1.6 deg) and found 0.21. The mean value from van Norren & Tiemeijer (1986) is 0.24; they also used larger fields (3.5 deg illumination, 2.5 deg detection).

Parameter 9. ILM reflectance

The ILM reflectance appeared to be low (0.26%). As judged from direct observation, the inner limiting membrane reflectance for this foveal site must be low compared to the high specular reflections in the perimacular region, which are particularly visible in young subjects. This is partly due to the surface being curved, which results in at most a very small specular reflection at the foveal pit. Values about 0.09 times the total outer segment disc reflection are indicative of low superficial stray-light at wavelengths greater than 500 nm.

Parameter 10. Media density

The lens density (0.54 at 420 nm, age dependent plus age independent part) for our group of subjects (average age 32, range 20 to 51 years) was lower than that reported by Pokorny *et al.* (1987) (0.73, also average age 32 years). The mean value from van Norren & Tiemeijer (1986) for four young subjects was 0.38 at 419 nm. Delori & Pflibsen (1989) found 0.66 for a group of 10 subjects aged between 22 and 38 years. Minor addition of media back-scatter to the data accounts for the data points at 410 and 430 nm being generally higher than the model fit. This backscatter also partly compensates for media losses when using reflection techniques, yielding lower values for the lens density than those obtained by using psychophysical techniques.

Absorption by water was responsible for the lower predictions for directional reflectance at long wavelengths [Fig. 1(c)]. Absorption of water is hardly recognized in the logarithmic representation of the original reflectance spectra.

Parameter 11. Media correction term

The media correction term, D_{ct}, was used only in the perpendicular, dark-adapted condition and is a measure of (for instance head position) stability during the measurement. Although generally positive, its value

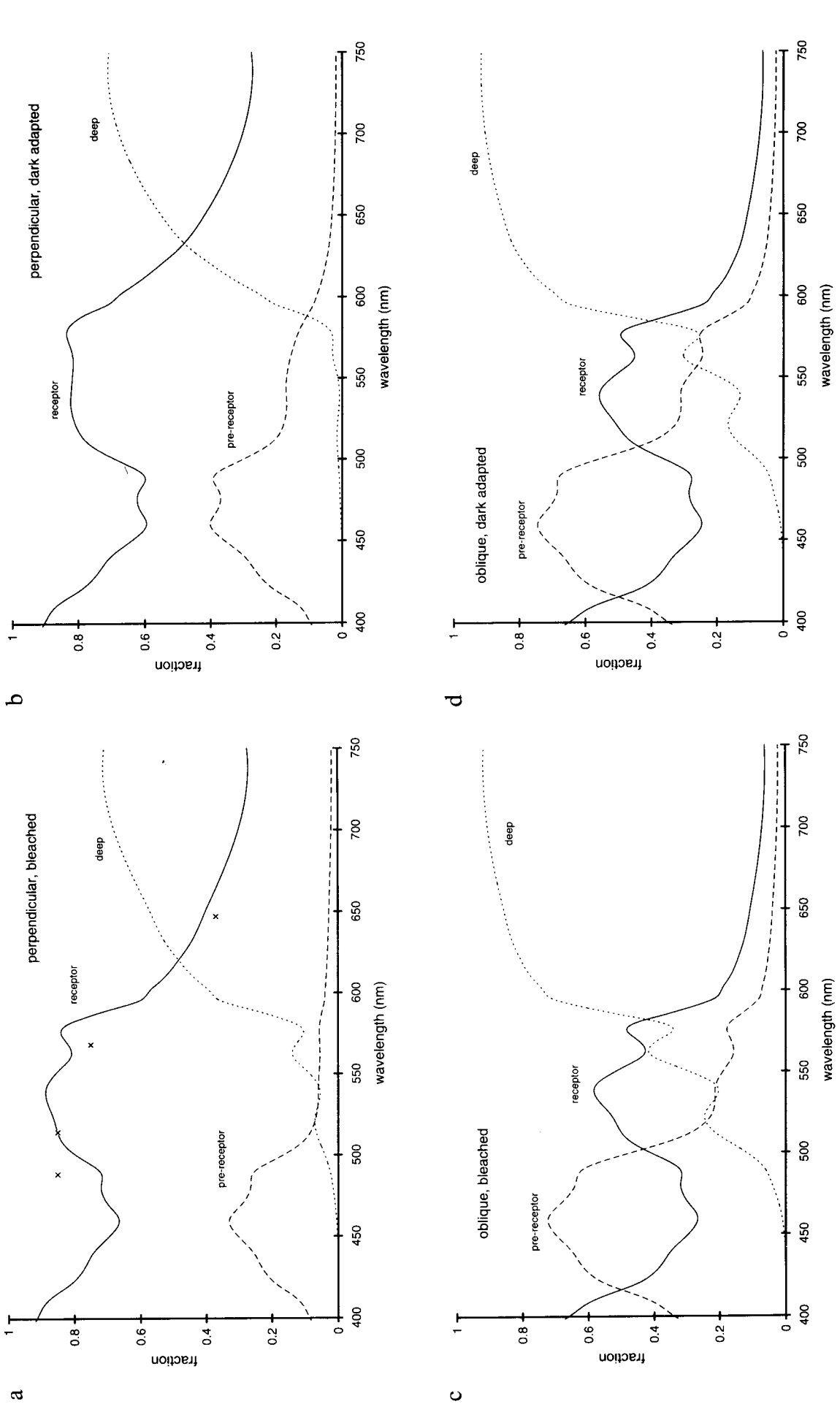

GR6.TIF

FIGURE 6. Model predictions of the fractional components of the different pathways. These components describe the four conditions measured in subject J.K. (a) bleached, perpendicular. (b) dark-adapted, perpendicular. (c) bleached, oblique. (d) dark-adapted, oblique. "Pre-receptor" represents all light reflected in front of the photoreceptors (ILM). "Receptor" represents the reflectance from the discs. "Deep" represents reflectance from the sclera. Crosses in (a) are the fractions with maintained polarization replotted from van Blokland (1986).

(0.018) is sufficiently low that no further comment need to be made. This leaves ten important free parameters.

Statistical analysis

Analysis of covariances between the 11 fitted parameters from a fit to the average subject spectral data yields insight into the degree of independence of the parameters. In addition, each parameter was stepped one by one over a range of fixed values, while the other parameters were allowed to vary. This cross-sectioning of the multi-dimensional parameter space yields (limited) insight into the occurrence of multiple minima. No multiple minima were found.

Only two covariances were significant, $D_{\text{lens-a}}$ with R_{disc} (0.75) and D_{mela} with D_{deepscat} (-0.83). The aging lens density hardly changed at wavelengths between 500 and 600 nm, where the (by definition) spectrally neutral R_{disc} is the most important component. It is yet unknown how this covariance is influenced by an underestimated lens density due to media backscatter. The negative covariance between melanin density, D_{mela}, and the density of deep scatter losses, D_{dscat}, means that the model is inclined to substitute the spectrally neutral density of D_{dscat} with the almost flat melanin spectrum at long wavelengths. As these are both parameters in our simplified modeling of the deeper layers, effects on receptor and pre-receptor layer parameters should be minimal.

Correlations between the fitted parameters were found by analyzing the parameters for the ten subjects. Age was added as an extra variable in the analyses. Only three correlation coefficients were higher than 0.7. The correlation between $D_{\text{lens-a}}$ and age (0.78) was expected. The correlation between SC and LWS coverage fraction LCOV (0.72) predicts lower directional sensitivity when a subject has a relatively high fraction of LWS cones. This is not very likely. In the long wavelength part of the spectrum, the model probably trades directly reflected light from LWS cones for deeper reflected light. The latter is also influenced by visual pigment changes but does not show directional sensitivity. The last high correlation (0.76) was R_{disc} with D_{vp}. This could simply mean that a longer outer segment has more discs, resulting in both higher total reflection and more visual pigment.

The three major components of reflected light

Once the total foveal reflectance has been put in a model, it is possible to show the underlying components. Plotted in Fig. 6 are the fractional contributions (as seen at the cornea) of the separate pathways; the ILM (pre-receptor), the discs (receptor), and the sclera (deeper layers). How the components behave as a function of wavelength in the four conditions is plotted in panels a, b, c and d. In Fig. 6(a), in the mid-spectral range, the pre-receptor fraction (the superficial stray-light component from the ILM) and the deeper fraction (sclera) are small; the receptor outer segment disc fraction accounts for almost 90% of the light emerging from the eye. At long wavelengths, the "deep" component dominates. Only this light has traveled the full layer of visual pigment twice (no leak in the perpendicular condition), as assumed in the simple model of the earliest densitometer studies. Dark adaptation of the visual pigments resulted in some loss of the receptor disc fraction around 550 nm, but also in an about a three-fold increase of pre-receptor reflected light [Fig. 6(b)]. This shows that "stray-light" in densitometry has an more important role in dark-adapted conditions. However, "stray-light" is even more important in the oblique conditions [Fig. 6 (c, d)], and the receptor signal only accounts for about 60% of the total reflection from the eye at mid-spectral wavelengths. This illustrates the importance of using small entry and exit pupils in instruments designed for optimal detection of light from the cone photoreceptors.

GENERAL DISCUSSION

Our model is the first to incorporate a directional reflection from the stack of discs in the outer segments of the photoreceptor. This has a major influence on the estimate of the density of visual pigment. We found calculated densities ranging from 0.41 up to 0.80, in agreement with psychophysical data. These values were much higher than the densities obtained using the simple model with a double traversion of the visual pigment layer. Our measured densities ranged from 0.32 to 0.54, with a mean of 0.44. With the simple model, assuming no stray-light, the estimated density for visual pigment is only 0.22. The graded density in our model is an important determinant in these higher values; stray-light from the ILM has only a minor effect. It should be emphasized that the magnitude of the directional receptor component strongly depends on the measuring technique used. Fundus reflectometers with large exit pupils, as used in older studies, do not make optimal use of the directional properties of the foveal cones. This results in shorter pathways through the photopigments and a higher stray-light fraction, hence lower measured visual pigment densities.

Several origins of the retinal reflections have been proposed in previous studies. Polarization, spectral decomposition, image quality of reflected light and visual pigment bleaching have been used as tools to discriminate between different layers. Campbell & Gubisch (1966) used white illumination light and concluded that the retina had a nearly perfect non-directional character. This is not very surprising, given the dominating reddish nature of the spectral reflectance of the deeper layers. There is now consensus that the reflection from deeper layers is red, has poor (aerial) image quality and destroyed polarization. The discussion is now concentrated on additional reflectors. Van Blokland (1986) measured the degree of maintained polarization of light from the fovea. His data, replotted in Fig. 6(a), show a striking resemblance to those for our receptor component. The decreasing polarization at longer wavelengths relates to the increasing fraction of deeper, unpolarized light. The reflection from the

receptor discs seems to maintain polarization. As argued in the Introduction, we do not agree with his interpretation of the RPE as the main origin of reflected light, as we assumed that all light that travels beyond the receptor layer has no directional properties. Earlier, Weale (1966) used polarization as well as visual pigment bleaching and reported reflections from Bruch's membrane with maintained polarization. The polarization state did not change much after visual pigment bleaching. This conclusion is supported by the relatively high receptor fraction in the dark-adapted condition, as can be seen in Fig. 6(b). Weale's experiments with different exit pupil sizes revealed that, consistent with our model, directional reflection occurred at mid-spectral wavelengths. Techniques that provide information supporting the receptor layer as an important reflector used the quality of the aerial image (Gorrand, 1985) and polarization (Rohler *et al.*, 1969) albeit without correction for retardation in the eye. In experiments in which adequate tools for discrimination are not used, the reflection from the receptors is easily confused with a reflection from the ILM (van Norren & Tiemeijer, 1986; Millodot, 1972; Charman, 1980) or RPE (van Blokland & van Norren, 1986).

Images of the fovea obtained with optical coherence techniques (Puliafito *et al.*, 1995) show a reflection from the region of the inner limiting membrane and relatively strong reflections in the region of the retinal pigment epithelium and choriocapillaris. Multiple scattering in the deeper layers is not detected with this technique. Similarly, distributed reflection along the depth of the outer segment may be underestimated. The use of IR wavelengths and entry and (large) exit pupils not aligned to the peak of the Stiles–Crawford maximum may further reduce the magnitude of the pronounced receptor component that we see with our instrument at wavelengths around 550 nm (Fig. 6). We suggest, in particular when looking at retinal detachment cases (for instance Puliafito *et al.*, 1995, case 9), that the double layer reflex near the RPE consists of a reflection from the outer segments and a reflection from, for instance, the choriocapillaris or Bruch's membrane. The comment made by the authors that the reflection at the receptors occurred due to "the normal incidence of the probing beam" is in full support of our theory about the origin of the directional reflection. In our model we include the reflection from the choriocapillaris and RPE region to the total of the non-directional reflectance from the deeper layers.

Using a laser slit lamp technique, Shahidi *et al.* (1990) found a double peaked reflection profile in the retina of normal human subjects. In the fovea, the reflection (543 nm) assumed to originate from the ILM region is about 30% of the reflection assumed to originate from the RPE region. The depth resolution of this technique is too low, however, to detect a gradual disc reflection.

The stack of discs in the outer segment has a resemblance to an ordinary Yagi-type television antenna. We think that both the discs and the Yagi elements influence the electromagnetic field in a similar way to achieve high forward sensitivity. The resulting increase in the average refraction index of the discs relative to the receptor interspaces forms the origin of the general wave guiding behavior (c.f. an optic fiber). We ignored the fact that the diameter of the outer segments of the receptor is small compared to the wavelength of light. Entering photons can be considered as Gaussian-shaped energy fields with, even when they enter perpendicular, some energy running in the interspace. On the other hand, interspace light may have some energy running in the outer segment. In the oblique condition, these factors cancel each other to a certain extent.

The advantages of receptor directionality include suppression of scattered light in the eye and efficient use of visual pigment in small cross-sectional outer segments, leaving an interspace for other purposes (supporting structures and transport). Our model does not require suppression of oblique light in an anatomically obscure absorber, shielding the visual pigment (Stiles & Crawford, 1933; van Blokland & van Norren, 1986). In addition, our model predicts that the light lost for vision is also lost for directional reflection. The directionality of the foveal reflectance is, however, more narrowly tuned than the one derived from psychophysical data. When fitted with a Gaussian curve, widths measured between the inflection points are found near 4.1 mm for the psychophysical data and 2.6 mm for reflection data (van Blokland, 1986). A possible explanation is that non-directional light reflected from deeper layers does not influence the width of the directional reflection data, while the part of the deeper reflected light traveling back through an outer segment broadens the width of the psychophysical data. Compare this with recapturing of light by neighboring receptors (Chen & Makous, 1989). Psychophysical data (Smith & Pokorny, 1973; Burns & Elsner, 1993; Pokorny & Smith, 1976) suggest that the peak density of visual pigment in LWS cones is higher than the peak density in MWS cones. We tried to consider both densities as free parameters, but could not find satisfactory solutions of the fitting process because of a high correlation between the LWS visual pigment density and the LWS coverage fraction. Perhaps the reddish nature of the deeper reflected light makes the LWS cones more efficient for visual perception.

At short wavelengths (<510 nm) the reflection from the ILM becomes an important stray-light factor, since light originating from the receptor layer is attenuated by the macular pigment. This forms an extra handicap if one tries to make densitometric measurements of the already sparse SWS cones. We estimated, using an extended version of our model containing SWS cones (not shown), that a measured density at 440 nm of only 0.015 can be expected for the SWS cones outside the very center of the fovea.

In summary, our model describes the spectral magnitude of the three main reflecting components in the human fovea, for different bleach levels and retinal angles. Separate pathways for directional reflection from

the foveal cone receptor discs and non-directional reflection from the pre- and post-receptor layers were found. This may be relevant to other techniques based on reflected light from the retina (for an overview of other techniques c.f. Knighton, 1995). The model yields estimates of the density of the visual pigments that are consistent with estimates based on psychophysical techniques. The model also yields estimates of the optical properties of other important absorbers. In spite of including the receptor layer with inherent refracting aspects, for the non-directional reflection from the deeper layers in bleached conditions it can still be ignored. As we simplified the modeling of these deeper layers, more complex modeling would be needed to arrive at physiologically relevant estimates for the parameters in the choroidal space.

REFERENCES

van Assendelft, O. W. (1970). *Spectroscopy of hemoglobin derivatives*. Springfield, IL: C. C. Thomas.

van Blokland, G. J. & van Norren, D. (1986). Intensity and polarization of light scattered at small angles from the human fovea. *Vision Research, 26*, 485–494.

van Blokland, G. J. (1986). Directionality and alignment of the foveal receptors assessed with light scattered from the human fundus. *Vision Research, 26*, 495–500.

Bone, R. A., Landrum, J. T. & Cains, A. (1992). Optical density spectra of the macular pigment *in vivo* and *in vitro*. *Vision Research, 32*, 105–110.

Burns, S. A. & Elsner, A. E. (1993). Color matching at high luminances: Photopigment optical density and pupil entry. *Journal of the Optical Society of America, 10*, 221–230.

Campbell, F. W. & Gubisch, R. W. (1966). Optical quality of the human eye. *Journal of Physiology London, 186*, 558–578.

Charman, W. N. (1980). Reflection of plane-polarized light by the retina. *British Journal of Physiological Optics, 34*, 34–49.

Chen, B. & Makous, W. (1989). Light capture by human cones. *Journal of Physiology, 414*, 89–109.

Cicerone, C. M. & Nerger, N. L. (1989). The relative numbers of long-wavelength-sensitive to middle-wavelength-sensitive cones in the human fovea centralis. *Vision Research, 29*, 115–128.

Coble, J. R. & Rushton, W. A. (1971). Stiles–Crawford effect and the bleaching of cone pigments. *Journal of Physiology, 217*, 231–242.

Curcio, C. A., Allen, K. A., Sloan, K. R., Lerea, C. L., Hurley, J. B., Klock, I. B. & Milam, A. H. (1991). Distribution and morphology of human cone photoreceptors stained with anti-blue opsin. *Journal of Comparative Neurology, 312*, 610–624.

Delori, F. C. & Pflibsen, K. P. (1989). Spectral reflectance of the human ocular fundus. *Applied Optics, 28*, 1061–1077.

DeMarco, P., Pokorny, J. & Smith, V. C. (1992). Full-spectrum cone sensitivity functions for X-chromosome-linked anomalous trichromats. *Journal of the Optical Society of America, 9*, 1465–1476.

Gabel, V. P., Birngruber, R. & Hillenkamp, F. (1978). Visible and near infrared light absorption in pigment epithelium and choroid. In Kyoto, Shimizu (Ed.) *XXIII Concilium Ophthalmologium* (Excerpta Medica). Amsterdam: Elsevier.

Gorrand, J. M. (1985). Directional effects of the retina appearing in the aerial image. *Journal Optics (Paris), 16*, 279–287.

Gorrand, J. M. & Delori, F. (1995). A reflectometric technique for assessing photoreceptor alignment. *Vision Research, 35*, 999–1010.

Hee, M. R., Izatt, J. A., Swanson, E. A., Huang, D., Schuman, J. S., Lin, C. P., Puliafito, C. A. & Fujimoto, J. G. (1995). Optical coherence tomography of the human retina. *Archieves of Ophthalmology, 113*, 325–332.

Hitzenberger, C. K. (1991). Optical measurement of the axial eye length by laser doppler interferometry. *Investigative Ophthalmology and Visual Science, 32*, 616–624.

Huang, D., Swanson, E. A., Lin, C. P., Schuman, J. S., Stinson, W. G., Chang, W., Hee, M. R., Flotte, T., Gregory, K., Puliafito, C. A. & Fujimoto, J. G. (1991). Optical coherence tomography for micron-resolution imaging. *Science, 254*, 1178–1181.

Jessop, G. R. (1971). *VHF-UHF Manual*. London: Radio Society of Great Britain.

King-Smith, P. E. (1973a). The optical density of erythrolable determined by retinal densitometry using the self-screening method. *Journal of Physiology, 230*, 535–549.

King-Smith, P. E. (1973b). The optical density of erythrolable determined by a new method. *Journal of Physiology, 230*, 551–560.

Knighton, R. W. (1995). Quantitative reflectometry of the ocular fundus. *IEEE Engineering in Medicine and Biology, 14*, 43–51.

Kraft, T. W., Makino, C. L., Mathies, R. A., Lugtenburg, J., Schnapf, J. L. & Baylor, D. A. (1990). *Cone excitations and color vision. Cold Spring Harbor Symposia on Quantitative Biology*, Vol *LV*.

Longhurst, R. S. (1973). *Geometrical and physical optics*. Hong Kong: Commonwealth Printing Press.

Miller, S. S. (1972). Psychophysical estimates of visual pigment densities in red–green dichromats. *Journal of Physiology London, 223*, 89–107.

Millodot, M. (1972). Reflection from the fundus of the eye and its relevance to retinoscopy. *Atti Fondatiore Georgi Ronchi, 27*, 31–50.

van Norren, D. & van de Kraats, J. (1981). Retinal densitometer with the size of a funduscamera. *Vision Research, 29*, 369–374.

van Norren, D. & Tiemeijer, L. F. (1986). Spectral reflectance of the human eye. *Vision Research, 26*, 313–320.

van Norren, D. & Vos, J. J. (1974). Spectral transmission of the human ocular media. *Vision Research, 14*, 1237–1243.

Packer, O., Hendrickson, A. E. & Curcio, C. A. (1989). Photoreceptor topography of the retina in the adult pigtail macaque. *The Journal of Comparative Neurology, 288*, 165–183.

Piket-May, M. J., Taflove, A. & Troy, J. B. (1993). Electrodynamics of visable-light interactions with the vertebrate retinal rod. *Optic Letters, 18*, 568–570.

Pokorny, J. & Smith, V. C. (1976). Effect of field size on red–green color mixture equations. *Journal of the Optical Society of America, 66*, 705–708.

Pokorny, J., Smith, V. C. & Lutze, M. (1987). Aging of the human lens. *Applied Optics, 26*, 1437–1440.

Polyak, S. L. (1941). *The retina* (p. 488). Chicago: University of Chicago Press.

Press, W. H., Flannery, B. P., Teukolsky, S. A. & Vettering, W. T. (1989). *Numerical recipes in Pascal*. Cambridge: Cambridge University Press.

Puliafito, C. A., Hee, M. R., Lin, C. P., Reichel, E., Schuman, J. S., Duker, J. S., Izatt, J. A., Swanson, E. A. & Fujimoto, J.G. (1995). Imaging of macular diseases with optical coherence tomography. *Ophthalmology, 102*, 217–229.

Ripps, H. & Weale, R. A. (1965). Analysis of foveal densitometry. *Nature London, 205*, 52–56.

Rohler, R., Miller, V. & Aberl, M. (1969). Zur messung der modulations-ubertragungs-funktion des lebenden menschlichen auges in reflektierten licht. *Vision Research, 9*, 407–428.

Rushton, W. A. H. (1965). Straylight and the measurement of mixed pigments in the retina. *Journal of Physiology, 176*, 46–55.

Shahidi, M., Zeimer, R. C. & Mori, M. (1990). Topography of the retinal thickness in normal subjects. *Ophthalmology, 97*, 1120–1124.

Smith, R. C. & Baker, K. S. (1981). Optical properties of the clearest natural waters. *Applied Optics, 20*, 177–184.

Smith, V. C. & Pokorny, J. (1973). Psychophysical estimates of optical density in human cones. *Vision Research, 13*, 1199–1202.

Snyder, A. W. & Pask, C. (1973). The Stiles–Crawford effect — explanation and consequences. *Vision Research, 13*, 1115–1137.

Stiles, W. S. & Crawford, B. H. (1933). The luminous efficiency of rays entering the eye pupil at different points. *Proceedings of the Royal Society B, 112*, 428–450.

Vos, J. J. & van Os, F. L. (1975). The effect of lens density on the Stiles–Crawford effect. *Vision Research, 15*, 749–751.

Vos, J. J. & Walraven, P. L. (1970). On the derivation of foveal receptor primaries. *Vision Research, 11*, 799–818.
Walraven, P. L. & Bouman, M. A. (1960). Relation between directional sensitivity and spectral response curves in human cone vision. *Journal of the Optical Society of America, 50*, 780–784.
Weale, R. A. (1966). Polarized light and the human fundus oculi. *Journal of Physiology, 186*, 175–186.
Wyszecki, G. & Stiles, W. S., (1982). *Color science: Concepts and methods, quantitative data and formulae*. New York: Wiley.

Acknowledgements—We thank Dr J. J. Vos, Professor V. C. Smith and Professor J. Pokorny for their critical comments on the manuscript.

APPENDIX

The directional reflectance data from van Blokland (1986) shows how reflected light from the receptors is concentrated to a Gaussian spot in the pupil plane. The weighted area under the two-dimensional Gaussian spot, with inflection points separated by S=2.6 mm, can be calculated as:

$$\pi \cdot S^2/2 = 10.6 \text{ mm}^2 \quad \text{(A1)}$$

For the area of a hemisphere centered at the retina, with the distance retina–pupil plane (16.7 mm) as a radius (r), we find:

$$2 \cdot \pi \cdot r^2 = 1750 \text{ mm}^2 \quad \text{(A2)}$$

The antenna gain is the ratio of the hemisphere area and Gaussian area, hence 165.

The diameter of the capture area is:

$$Gain \cdot \lambda/(4 \cdot \pi) = 165 \cdot 0.55^2/(4 \cdot \pi) = 4 \ \mu\text{m} \quad \text{(A3)}$$

Thus, with inner segment diameters of foveal cones of about 2.5 μm (Polyak, 1941; Packer *et al.*, 1989), the capture area of a single cone is indeed larger than the physical area of the inner segment. Cones are tightly packed in the fovea, we assume therefore that light does not enter the cone interspaces directly.